Γ_s = surface concentration in stagnant film, moles/sq.cm.
δ = thickness of the water layer, cm.
μ = liquid viscosity, g./cm. sec.
Π = film pressure, dynes/cm.
τ = shear stress at surface, dynes/sq.cm.

LITERATURE CITED

1. Cullen, E. J., and J. F. Davidson, *Trans. Faraday Soc.*, **53**, 113 (1957).
2. ———, *Chem. Eng. Sci.*, **6**, 49 (1956).
3. Danckwerts, P. V., and A. M. Kennedy, *ibid.*, 8, 201 (1958).
4. Davies, J. T., and E. K. Rideal, "Interfacial Phenomena," Academic Press, New York (1961).
5. Kunin, R., "Ion Exchange Resins," 2 ed., Wiley, New York (1958).
6. Levich, V. G., "Physicochemical Hydrodynamics," Prentice-Hall, Englewood Cliffs, New Jersey (1962).
7. Lynn, S., J. R. Straatemeier, and H. Kramers, *Chem. Eng. Sci.*, 4, 49, 58 (1955).
8. Merson, R. L., Ph.D. thesis, Univ. of Illinois, Urbana, Illinois (1964).
9. ———, and J. A. Quinn, *A.I.Ch.E. Journal*, **10**, No. 6, 804 (1964).
10. Nijsing, R. A. T. O., R. H. Hendriksz, and H. Kramers, *Chem. Eng. Sci.*, **10**, 88 (1959).
11. Ratcliff, G. A., and K. J. Reid, *Trans. Inst. Chem. Engrs. (London)*, **39**, 423 (1961); **40**, 69 (1962).
12. Savic, P., "Circulation and Distortion of Liquid Drops Falling Through a Viscous Medium," National Research Council of Canada, Report No. MT-22 (1953).
13. Wendel, M. M., Ph.D. dissertation, Univ. of Delaware, Newark, Delaware (1956).

Manuscript received August 4, 1964; revision received October 12, 1964; paper accepted October 14, 1964.

Longitudinal Dispersion in Pulsed Perforated-Plate Columns

TERUKATSU MIYAUCHI and HARUHIKO OYA

University of Tokyo, Tokyo, Japan

Experimental measurements have been performed for pulsed perforated-plate columns of different sizes and geometry to obtain longitudinal dispersion coefficients for continuous and dispersed phases and size and holdup of liquid droplets dispersed in the columns. These quantities are correlated with operating conditions and column design, including the data published by different authors. Longitudinal dispersion coefficients for the continuous phase are shown to follow the backflow model. A superficial number of stages in series in each compartment is shown to come from inherent instability of fluid motion in the compartment. The longitudinal dispersion coefficient of the dispersed phase approaches that of the continuous phase with increasing pulse velocity. Holdup and mean size of droplets are correlated mainly on the basis of the rate of energy dissipation in the column fluid. Inclusion of dispersed-phase viscosity is shown to correlate the holdup data successfully for different liquid-liquid systems.

Many investigations have been presented for pulsed perforated-plate columns since Van Dijck's first presentation of this type of extractor (*35*) and successful application of it to the reprocessing of spent reactor fuel at Idaho and Oak Ridge. Of these, some experimental works (*4, 5, 26*) have revealed that column HTU takes a minimum value with increasing pulse frequency and amplitude. Influence of longitudinal dispersion on column behavior is mentioned in the works by Thornton (*32*) and others.

This paper presents the column behavior along the theoretical treatment presented recently (*17, 18, 20, 21,* 29) for two-phase counterflow operations with longitudinal dispersion. The theory seems particularly helpful to interpret extraction-rate data obtained in continuous countercurrent extraction columns. Dimensionless parameters are included to characterize the behavior: individual column Peclet numbers for each phase to specify the extent of longitudinal dispersion, true overall NTU to characterize the rate of local mass transfer, and capacity ratio (extraction factor). Of these parameters longitudinal dispersion behavior of pulsed perforated-plate columns is presented here on the basis of experimentally measured dispersion coefficients. Burger and Swift (*3*) and Mar and Babb (*16*) have reported longitudinal dispersion coefficients obtained by measuring concentration pattern of steadily injected tracer material, and Eguchi and Nagata (*7*) have presented those calculated from extraction runs. Miyauchi and Vermeulen (*22*) show that the coefficients are well correlated on the basis of backflow.

Correlation of the dispersed-phase holdup is also included here, since this quantity has an intimate relation with longitudinal dispersion coefficient and local mass transfer behavior of this phase. Experimentally measured holdup data are also available from Cohen and Beyer (*5*), Thornton (*32*), and Sehmel and Babb (*25, 27*).

EXPERIMENTAL APPARATUS AND PROCEDURES

Experimental Apparatus

The assembly of the entire apparatus is shown in Figure 1. It consists of constant level feed vessels for water, methyl isobutyl keton (MIBK), and 0.1 N aqueous solution of potassium chloride as tracer electrolyte; and a pulse perforated-plate

Haruhiko Oya is with Showa Denko Company, Ltd., Tokyo, Japan.

TABLE 1. DIMENSIONS OF PULSED PERFORATED-PLATE COLUMNS

Inside diameter of column	D_T (mm.)	: 32, 54
Effective height of column*	L (mm.)	: 370, 780, 860
Compartment height	L_o (mm.)	: 10, 12.5, 20, 25, 30, 40, 50, 70, 100
Hole diameter of perforation	d_h (mm.)	: 1.5, 3.0
Plate thickness	(mm.)	: 1.60 (s.s.), 1.00 (Brass)
Free area of perforated plate	m (%)	: 9.5, 19.0
	Range of operational variables	
Flow rate : Water	$\overline{F}_c$ (cm./sec.)	: See Figures 2 and 4
MIBK	$\overline{F}_d$ (cm./sec.)	: See Figures 2 and 4
Linear amplitude of pulsation†	l (cm.)	: 0 ~ 1.5
Frequency of pulsation	ω (cycles/sec.)	: 0.4 ~ 3.0
Holdup of dispersed phase	ϵ_d (%)	: 0 ~ 25

* Distance between top and bottom plates.
† The amplitude is the value averaged over the cross-sectional area of the column.

column, a pulse generator of the plunger-displacement type, platinum electrodes for detecting concentration change of tracer electrolyte, 1.0 KC a.c. oscillator, an amplifier for measuring electrodes-circuit current, a CdS photoconductor probe combined with a light source, and a pen-writing recorder.

Pulse Column

Dimensions of the pulsed perforated-plate columns utilized in the runs are summarized in Table 1. The smaller diameter columns consist of double concentric borosilicate glass pipes. The inside diameter of outer pipe has the same dimension with the outer diameter of inner pipe. The outer pipe has dimensions of 3.5 cm. I.D. and 37 cm. (shorter column) or 78 cm. (longer column) in length. Inside the pipe are located glass spacer rings of the same dimensions. These rings constitute the inside pipe, being located in series to support a perforated plate between each ring. Dimensions of the ring are 3.5 cm. O.D., 3.2 cm. I.D., and variable in axial ring height (this height is equivalent to one compartment height L_o). The larger diameter column consists of a brass pipe of 5.4 cm. I.D. and 86 cm. in length. A stainless steel spacer of 1.0 cm. O.D. is located axially to support the perforated plates.

Two taps with an inside diameter of 2.0 cm. are installed at the bottom and middle positions of the columns for inserting electrical conductivity probes.

Droplets disengaging chambers at the top and bottom of the columns have dimensions of 5.8 cm. I.D. and 35 cm. in axial length.

MIBK phase (dispersed) is introduced to the bottom section of the column through a stainless steel pipe. The outlet distributor of the pipe is located at 80 mm. down below the bottom perforated plate and consists of a perforated plate of 25-mm. diameter with three 3.0-mm. holes and one central 5.0-mm. hole surrounded by the smaller holes.

Pulse Generator

A reciprocating plunger type of pulsator is utilized. The diameter of the plunger is 30 mm., and the stroke is variable between 0 to 9.0 cm. Pulsation from the pulsator is transmitted to the column liquid through the bottom flange.

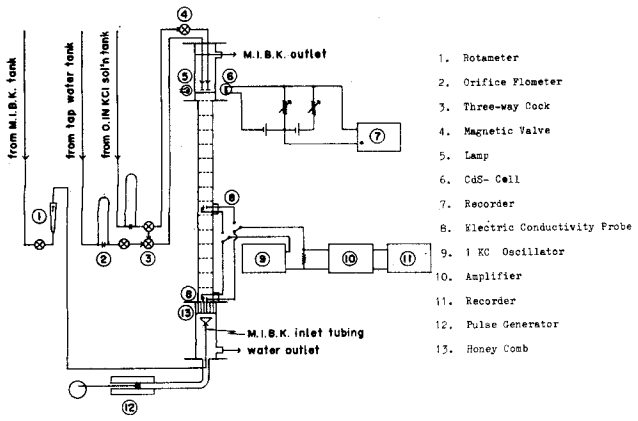

Fig. 1. Schematic diagram of pulsed perforated-plate column and electrical measuring devices and measurement system.

Perforated Plates

The plates are made of stainless steel or brass, and have circular perforation arranged in equilateral-triangular position. The free area of the perforation is given in Table 1.

Tubing

All the MIBK lines are glass tubing connected with polyethylene tubing to avoid contamination due to high molecular weight materials. A magnetic value regulates the flow quantity of aqueous potassium chloride solution introduced to the column as the tracer.

Concentration Measurement

The concentration of aqueous potassium chloride solution is measured continuously by electrical conductivity method, and the time variation of the conductivity is recorded continuously. The electrical conductivity probe consists of two equivalent platinum plates covered with platinum black. The plate is 10 × 10 sq. mm. and is placed 5 mm. apart. Liquid flow through the probe is entirely free.

Bottom Disengaging Section

A honeycomb of 5-mm. ϕ openings and 70 mm. in axial length is placed axially in the upper part of the bottom disengaging section (see Figure 1) to ensure the boundary condition, Equation (3). The conductivity probe is placed on the bottom plate. This honeycomb device, however, is only utilized for single-phase flow runs and not for two-phase counterflow runs to avoid preferential flooding at this section. In the latter case the probe is located in the midsection of the column, since the boundary condition, Equation (3), is not exactly satisfied at the bottom plate end.

Experimental Procedures

When the flow condition of aqueous continuous phase (for single-phase flow) or that of countercurrently flowing continuous aqueous and dispersed MIBK phases (for two-phase counterflow) reaches steady state, the aqueous potassium chloride solution is introduced into the continuous aqueous stream at its inlet as a concentration impulse through the magnetic value. Concentration change at the location of the conductivity probe is then recorded continuously to obtain the concentration response to the impulse. The response curve is compared with the theoretical ones for the diffusion model, and longitudinal dispersion coefficient for the continuous phase is determined on the basis of the model. Details of the procedures are given elsewhere (*19, 23*), and the range of the operating variables is shown in Table 1.

For measuring an effective longitudinal dispersion coefficient for the dispersed MIBK phase, MIBK solution of oil-soluble red color dyestuff is utilized as tracer material. A concentration impulse for the dispersed phase is introduced at the MIBK inlet distributor by injecting 1 to 3 cc. of the solution during the lapse of time within 5% of the mean residence time of the dispersed phase. The concentration response of the dispersed phase is measured at the section slightly lower or higher

than the droplets separating interface in the upper disengaging section, where the interface is maintained at the position by one compartment height higher than the top plate. The concentration response is measured photoelectrically and is recorded continuously. The effective longitudinal dispersion coefficient is obtained from the response curve on the basis of the diffusion model as stated later.

Droplet holdup is measured volumetrically by closing all the incoming and outgoing streams simultaneously and observing the increase of dispersed MIBK-phase volume at the droplet-separating interface in the upper disengaging section.

ANALYSIS OF RESPONSE CURVES

To obtain the longitudinal dispersion coefficient for ith phase ($i = c$ and d), the one-dimension diffusion-model approach is utilized here, which assumes a mean longitudinal dispersion coefficient E_i and a mean flow rate F_i. The basic transient equation is (6)

$$\partial c_i/\partial\theta = E_i\,\partial^2 c_i/\partial z^2 - F_i\,\partial c_i/\partial z \quad (i = c \text{ and } d) \quad (1)$$

Boundary conditions for the ith phase appropriate to the countercurrent flow operations with high intensity of fluid mixing in the main column are as follows:

$$z = 0: -E_i\,(\partial c_i/\partial z)_{z=0+} = F_i\,(c_i^{\circ} - c_{i,z=0+}) \quad (2)$$

$$z = L: -E_i\,(\partial c_i/\partial z)_{z=L-} = 0 \quad (3)$$

where the inlet-side plate for the ith phase is taken as the origin for axial distance z. The initial conditions depend upon what kind of experimental method is utilized to find the dynamic response of the column.

The delta-response solution to Equation (1) under the above boundary conditions is available in the exact form (*13, 37*) or in approximate forms (*2, 10, 14*). Also extensive numerical tables are available from the literature (*10, 13, 37*). Longitudinal dispersion coefficients for continuous and dispersed phases are determined from the lapse of time to reach the maximum concentration value for the response curve when the column Peclet number $\lesssim 8$, and the maximum concentration value when the Peclet number $\gtrsim 10$.

When the electrical conductivity probe is placed at the midheight of the column, the response curve is analyzed on the basis of the solution by Aris and Amundson (*1*) for a semi-infinite column. Details of measuring longitudinal dispersion coefficient are reviewed elsewhere (*19*).

RESULTS OBTAINED

Experiments have been performed to measure longitudinal dispersion coefficients for continuous and dispersed phases, droplet holdup in the main column, and droplet size by photographic method. The experimental liquid-liquid system is confined to the water-MIBK system, where MIBK is always dispersed into water.

LONGITUDINAL DISPERSION COEFFICIENT FOR CONTINUOUS PHASE

Based on the backflow model approach, Miyauchi and Vermeulen (*22*) have presented the following equation for the emulsion type of operation in the sense of Sege and Woodfield (*26*):

$$\frac{E_i/\epsilon_i}{\omega l L_o} = \frac{\bar{F}_i/\omega l \epsilon_i}{2\beta - (1/n_p)} + \frac{1}{\beta} \quad (4)$$

β is defined as a superficial number of perfectly mixed stages in series in each compartment and shown (22) to be commonly between 1 and 2 for the continuous phase coefficients. Experimental correlation of β is tried further as follows.

Single-Phase Flow

Volume fraction ϵ_c of continuous aqueous phase is 1.0 under zero flow rate of dispersed MIBK phase. An empirical dimensionless expression for β which correlates the experimental data reasonably well for various column designs is obtained as follows:

$$\beta = 0.57\,(D_T^2 L_o)^{1/3}/(d_h/m) \quad (5)$$

Figure 2 compares the experimental E_c values (open mark) with those calculated from Equations (4) and (5), where $1/n_p$ included in Equation (4) is neglected in comparison with 2β. As is stated in the discussion section, the correlation, Equation (5), should be considered as a first approximation.

Two-Phase Counterflow

Experimentally obtained E_c/ϵ_c for steady two-phase counterflow runs are also summarized in Figure 2 (black mark) for various column designs. Equations (4) and (5) again correlate the data reasonably well, showing that

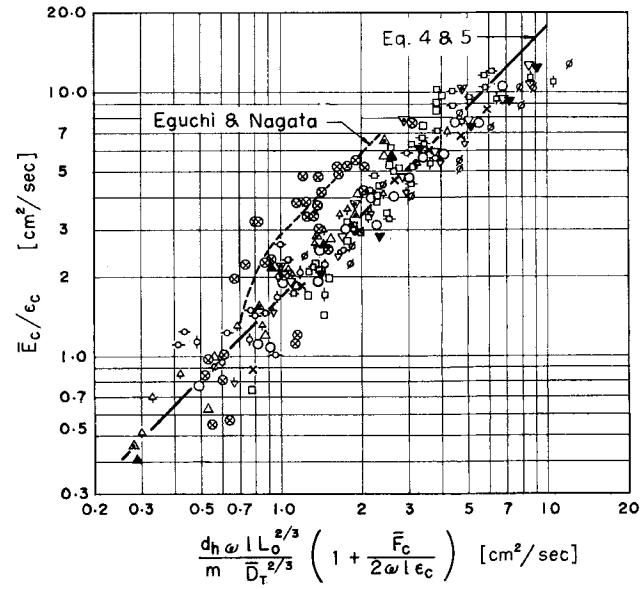

Fig. 2. Longitudinal dispersion coefficients for continuous phase, $\bar{F}_c/\epsilon_c$ compared with Equations (4) and (5).

	Measured at mid section of the column					✳	Eguchi & Nagata[7]
m	0.095	0.19					0.081
D_T	3.2						5.8
d_h	0.15						0.15
L_o \ F_d	0.0				0.043	0.0	0.18~0.38
1			△ (0.17)		▲ (0.30)	△ (0.26)	
1.25			△ (0.05)				
2						□ (0.06~0.59)	
2.5			□ (0.052~0.057)				
3						▽ (0.27)	
4						× (0.27)	
5	○ (0.053~0.055)	○ (0.049~0.054)	⌀ (0.06~0.14)			○ (0.27)	⊗ (0.151~0.442)
7				▽ (0.17)	▼ (0.45)	▽ (0.27)	
10						□ (0.27)	

Symbols used in Figure 2. Figures in parentheses are for F_c cc./(sq. cm.)(sec.).
*Measured at bottom section of the column.

* Tabular material has been deposited as document 8255 with the American Documentation Institute, Photoduplication Service, Library of Congress, Washington 25, D. C., and may be obtained for $2.50 for photoprints or $1.75 for 35-mm. microfilm.

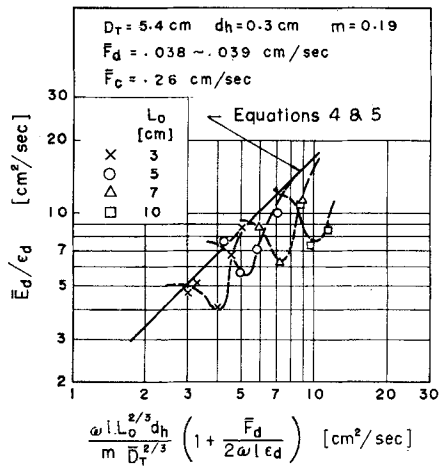

Fig. 3. Longitudinal dispersion coefficient for dispersed phase $\bar{F}_d/\epsilon_d$ compared with Equations (4) and (5).

there is no particularly different flow mechanism between single-phase flow and two-phase counterflow.

LONGITUDINAL DISPERSION COEFFICIENT FOR DISPERSED PHASE

Experimentally obtained E_d/ϵ_d for steady two-phase counterflow runs is shown in Figure 3 for various compartment heights, where the parameter with Figure 2 is taken. When the compartment height is fixed, E_d/ϵ_d is seen to approach to the line calculated from Equation (4) with increasing pulse velocity ωl, where Equation (5) for β is introduced to Equation (4). This suggests that flow behavior of the dispersed MIBK phase approaches steadily an ideal backflow model with increasing pulse intensity.

CORRELATION OF DROPLET HOLDUP

Droplet holdup data are correlated for the runs of measuring longitudinal dispersion coefficients of dispersed and continuous phases, dissolution rate of MIBK droplets into aqueous continuous phase, and extraction rate of *n*-butyric acid by continuous aqueous phase from the dispersed MIBK phase. As is stated in the discussions, the term $\epsilon_d/F_d^{2/3}$ has semiempirically turned out proportional to $\omega l/L_o^{1/3}$. This proportionality relation is further extended to cover the various authors' holdup measurements for different liquid systems. The final correlation is obtained as follows:

For

$$\psi \equiv \frac{\omega l}{(\beta_c L_o)^{1/3}} \cdot \left(\frac{\mu_d^2}{\sigma \Delta\rho}\right)^{1/4} < 0.21$$

$$\epsilon_d/F_d^{2/3} = 0.66\,\psi^{0.84} \qquad (6)$$

and for $\psi > 0.21$

$$\epsilon_d/F_d^{2/3} = 6.32\,\psi^{2.4} \qquad (7)$$

Figure 4 compares Equations (6) and (7) with the experimental holdup data covered here.

MEAN DROP DIAMETER

The mean drop diameter of dispersed MIBK droplets is measured photographically for 54-mm. diameter column at its cross section slightly above the top perforated plate in the upper disengaging section. Water is filled between the outer surface of the glass wall of the disengaging section, and a glass plate is attached to the wall, thus avoiding optical distorsion of the droplets images due to the curvature of the glass wall. 35-mm. camera with an $f = 2.0$ and 50 mm. focal length lens is used. An extension tube is attached to the lens to get desired magnification. A strobolight is used as a light source at the flash duration of 45 μsec.

The mean drop diameter $\bar{d}_p$ is determined by

$$\bar{d}_p = \Sigma\, n\, d_p^3 / \Sigma\, n\, d_p^2 \qquad (8)$$

where n is always more than fifty drops or more, and the individual diameters d_p are measured on enlarged photoprints. Flow rate of the MIBK-phase is maintained at a constant value of 0.043 cc./sq. cm. sec.

As is stated later in the discussions, the mean drop diameter has turned out well correlated by the following relation as shown in Figure 5:

$$\omega l/L_o^{1/3} > 1.2 : \bar{d}_p = 0.081\,(\omega l/L_o^{1/3})^{-1.2} \qquad (9)$$

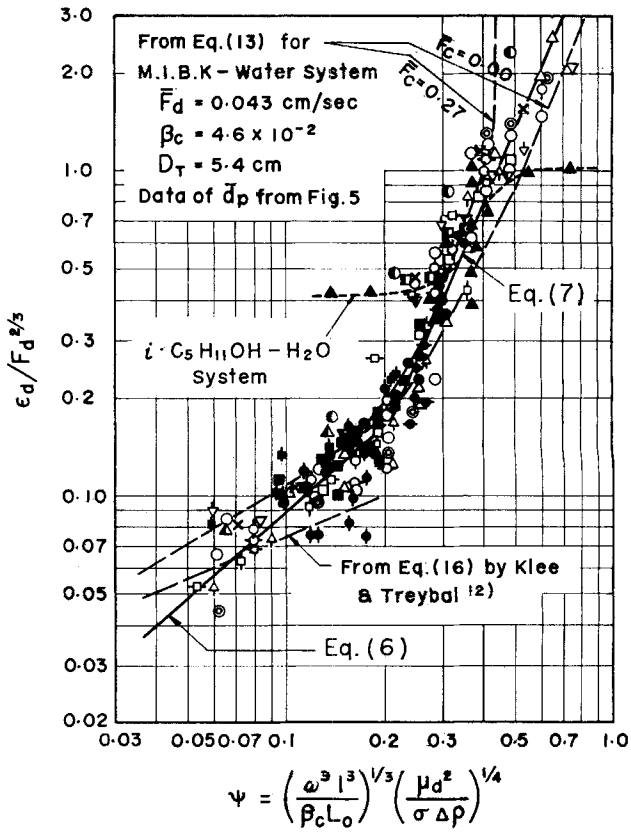

Fig. 4. Holdup data compared with Equations (6) and (7).

Dispersed phase	M. I. B. K.							Benzene		Toluene	Hexane	Isoamyl Alcohol
	Measurement of $\bar{E}_c$ & $\bar{E}_d$	Dissolution	Extraction				Sehmel & Babb [27]	Sehmel & Babb [27]	Shirotuka et al [28]	Li & Newton [15]	Sehmel & Babb [27]	Cohen & Beyer [9]
L_o \ $\bar{F}_d$	.043	.027	.02	.033 ~ .042	.075	.135	.260	.173, .260	.04	.275, .375	.173, .260	.172
1	▽			△								
2			◎	○	◇	◇						
3	▽	◐		×								
4				□								
5	▽	▲		△			●	■			●	▲
5.7										●		
7	◧			◇								
10	◧			◇								
12									●			
$\bar{F}_c$	.30, .45	.10 ~ .27	.264	.264	.264	.264	.260	.173, .44	.22	.32 ~ .49	0 ~ .44	.035
σ	dyne/c.m.	10.3						32.2		36.0	38.8	4.8
Δρ	g/cu. c.m.	0.204						0.129		0.129	0.348	0.192
μ_d	g/c.m. sec.	0.554 × 10⁻²						0.580 × 10⁻²		0.586 × 10⁻²	0.287 × 10⁻²	4.36 × 10⁻²

Symbols used in Figure 4.

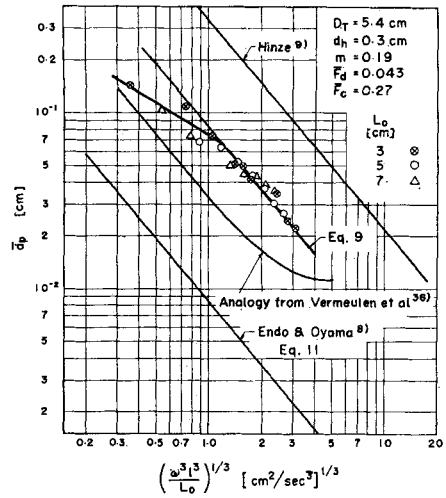

Fig. 5. Comparison between droplet diameters measured and those calculated from the use of various authors' correlations.

For $\omega l/L_o^{1/3} < 1.2$, $\bar{d}_p$ deviates gradually from the above relation, reducing the power in its absolute value from -1.2 to -0.6. The data, however, are not enough to ensure the relation.

DISCUSSION

Longitudinal Dispersion Coefficients

Physical meaning of β is considered closely related to the instability of liquid motion in a given stage. As a first approximation, the geometrical structure of a compartment is assumed to be of prime importance. The empirical correlation, Equation (5), is obtained with this premise. In accordance with the experimental observations, β becomes somewhat larger in general with increasing l, $\bar{F}_c$, and $1/\omega$, respectively. The influence of these variables, however, seems of secondary importance for β.

Figure 6 shows photographs which illustrate the physical meaning of β, that is how the fluid motion in a compartment looks when $\beta \approx 1$ or 2. To show the fluid motion in the column, a small quantity of benzene solution of carbon tetrachloride is dispersed as tracer droplets into the continuous water phase. The density of the tracer solution is adjusted at the density same with water. A 500-w. photo flood lamp is used as a light source, and the photographs are taken at about the midheight section of the column.

When $\beta \approx 1$ ($L_o = 2$ cm. for the present case), a single tori type of vortex is formed in each compartment, and for $\beta \approx 2$ ($L_o = 5$ cm. for the present case) two tori types of vortices are formed in series in each compartment. In the latter case one compartment behaves as if it were nearly two compartments in series. Apparently the vertex motion in each compartment maintains the motion throughout the pulse cycles.

For $L_o = 3$ cm., vortex formation is somewhat unstable. The number of vortices in series depends on pulse condition, sometimes forming single vortex, two vortices in series, or one vortex plus another imperfect vortex. For $L_o = 7$ cm., two vortices are formed, the one at the upper part of a compartment and the other at the lower part of it. Apparently definite vortex formation is not observed for the fluid between these two vortices, and this stagnant fluid portion elongates in its axial length with increasing stage height L_o.

The data by Eguchi and Nagata (7) deviate from the present correlation as shown in Figure 4. One possible reason may be ascribed to their assumption that the dispersed phase flows in piston flow manner, thus giving higher values for $\bar{E}_c$.

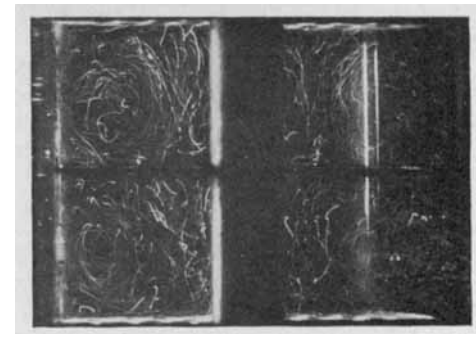

Fig. 6a. Photograph illustrating fluid motion in compartments when $\beta \approx 1$; experimental conditions are $D_T = 5.4$ cm., $L_o = 2$ cm., $l = 0.9$ cm., $\omega = 3$ cycles/sec., and time of exposure = 1/15 sec.

Longitudinal dispersion coefficients for the dispersed phase, Figure 3, show clearly a minimum point with increasing pulse velocity. The left-hand side branch of the minimum point is considered to come from the Taylor's velocity distribution mechanism (*31*) due to drop size distribution. This reasoning is justified because Taylor's mechanism becomes predominant with an increase in the compartment height L_o, where mean drop size becomes greater and drop size distribution wider, both with increasing L_o under a constant pulse velocity.

As mentioned previously, the right-hand side branch shows that droplet motion becomes random with increasing pulse velocity and approaches steadily the mixing behavior of the continuous phase.

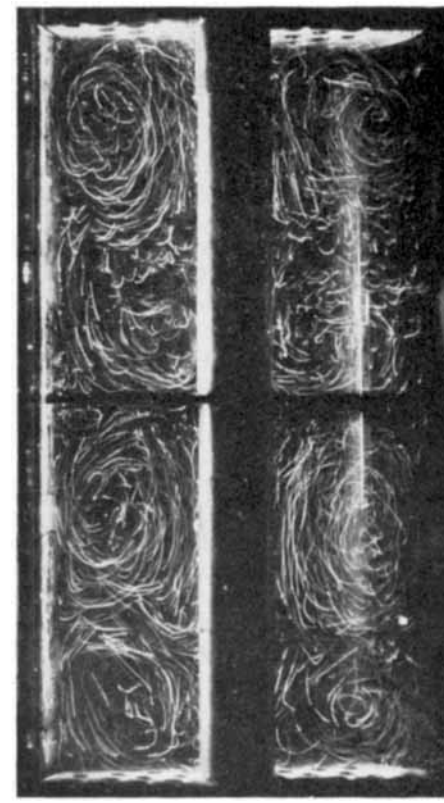

Fig. 6b. Photograph illustrating fluid motion in compartments when $\beta \approx 2$; experimental conditions are $D_T = 5.4$ cm., $L_o = 5$ cm., $l = 0.9$ cm., $\omega = 3$ cycles/sec., and time of exposure = 1/15 sec.

Mean Drop Size

When the flow condition of the mixed phases in a pulsed perforated-plate column is under a developed turbulent condition, fluid dynamic behavior of the mixed phases is considered governed by the mean rate of energy dissipation per unit mass of the mixed phases.

Under the premise that the concept of Kolmogoroff's local isotropy is applicable to drop dispersion in a mixing vessel, Endō and Oyama (*8*) presented the following empirical equation for mean drop size of dilute liquid-liquid suspension :

$$\bar{d}_p/\lambda_o = 1.73 \cdot 10^{-2} (\sigma\lambda_o/\rho\nu^2)^{3/5} \qquad (10)$$

where λ_o takes the following form:

$$\lambda_o = (\nu^3/\bar{\epsilon}_o)^{1/4}$$

Equation (10) is for steady state dispersion and enables one to calculate $\bar{d}_p$ by knowing $\bar{\epsilon}_o$, where the empirical equation is reported applicable to the range of $\bar{d}_p/\lambda_o \gtrsim 1$.

$\bar{\epsilon}_o$ for a pulsed perforated plate column is calculated from Equation (A4) (see Appendix), and hence $\bar{d}_p$ is determined for the same column under the premise same with the above authors. When one takes $\gamma_c = 9.4$ for Equation (A-4), $\sigma \doteqdot 10.3$ dyne/cm., and $\rho_m \doteqdot \rho_c = 1.0$ g./cc. for dilute MIBK-water system, $\bar{d}_p$ is approximately expressed as follows:

$$\bar{d}_p \approx 8.3 \cdot 10^{-3} (\omega l/L_o^{1/3})^{-1.2} \qquad (11)$$

From the magnitude of empirical mean drop size, the value of $\bar{d}_p/\lambda_o$ is in the range of the 6 to 9. Equation (11) is plotted in Figure 5 as a reference. It is seen that the empirical mean drop size is about ten times greater than that calculated from Equation (11). The same tendency is also observed in the authors' unpublished work on the mean drop size in a rotating disk type of extractor for the same system. The mean drop size calculated from the correlation by Hinze (*9*) for the maximum stable drop size is also shown in Figure 5, along with the mean drop size calculated from the correlation by Vermeulen and co-workers (*36*). The latter correlation is for agitated vessels and is formally reduced to the functional relationship shown in Equation (10).

These curves differ from one another, and the difference suggests that the droplet dispersion process in the column is not steady, but rather the droplets are unsteadily dispersing into smaller ones, or the extent of droplet coalescence of this particular liquid system is rather high. In accordance with the experimental observation by Vanderveen (*31*), impeller tip drop size for MIBK-water system in an agitated vessel is reported in good agreement with the correlation by Vermeulen et al. (*36*), but the drop size increases gradually with distance from the tip and finally reaches to about several to ten times greater than the tip size. The above two mechanisms are perhaps responsible for this observation.

In spite of the complicated mechanisms and uncertainties for droplet dispersion in the pulse columns, it is somewhat surprising that the term $(\omega l/L_o^{1/3})$ to the power -1.2 agrees well with that calculated from the correlations for steady dispersion.

A convenient method to determine a mean drop size easily calculable is to assume that the drop moves freely as a solid sphere at its terminal velocity through surrounding fluid, and all the droplets have equal drop size. With these assumptions, the mean travelling velocity of the droplets relative to counterflowing continuous phase is given by

$$\bar{u}_t = |\bar{F}_d/\epsilon_d| + |\bar{F}_c/(1-\epsilon_d)| \qquad (12)$$

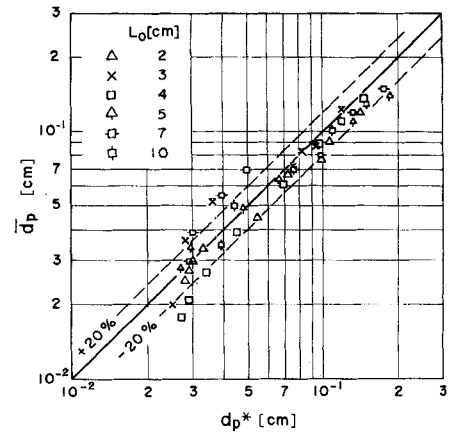

Fig. 7. Comparison between d_p^* (calculated) and $\bar{d}_p$ (measured).

$\bar{u}_t$ affords, in turn, a mean drop size d_p^* corresponding to the above assumption from known physical properties of the liquid system. Figure 7 shows the relation between $\bar{d}_p$ and d_p^* thus calculated, where $\bar{d}_p$ is the mean drop size read from the experimental average curve in Figure 5. d_p^* is seen nearly equal to $\bar{d}_p$.

Since d_p^* is easily calculable from known volume fraction of the dispersed phase in the main column, local mass transfer coefficient calculated on the basis of d_p^* will give useful information provided that the mechanism of overall mass transfer is known between a droplet and surrounding fluid.

Droplet Holdup

Thornton et al. (32) have correlated the holdup of dispersed phase on the basis of characteristic velocity. Sehmel and Babb (*27*) report that holdup does not change appreciably with the flow rate of the continuous phase.

A correlation based on the characteristic velocity is tried for the present case, but the data correlated scatter for the region of intensive pulsation of $\omega l/L_o^{1/3}$ greater than 1.2 as shown in Figure 8.

The observation that ϵ_d is proportional to $\bar{F}_d^{2/3}$ and not to $\bar{F}_d$ is considered to come from the two possibilities that droplet dispersion is not steady, but rather unsteadily dispersing during travel through the column, or droplet coalescence becomes noticeable where these two possibilities are considered to become noticeable with increasing $\bar{F}_d$.

Now the discussion will be turned to the correlations for droplets holdup shown in Figure 4. As a simplest approach first assume that the droplets behave as if they

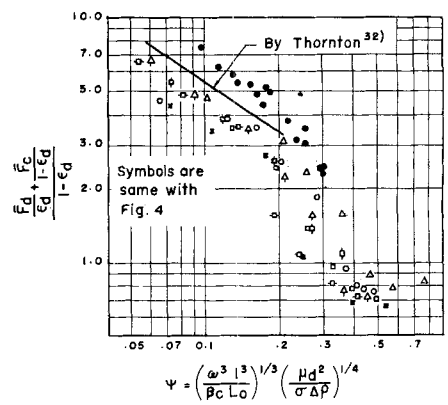

Fig. 8. Correlation based on the characteristic velocity (MIBK-water system).

were solid spheres travelling freely at the terminal velocity through the continuous medium. With these assumptions, the terminal travelling velocity u_t of the droplets with a mean diameter d_p is expressed by

$$\bar{u}_t = \sqrt{\frac{4\,g\,d_p\Delta\rho}{3\,f\,\rho_c}} \tag{13}$$

Re_p calculated for the droplets in the present runs ranges from Stokes to Allen regions.

For the Stokes region apply Equation (9) to d_p included in Equation (13) and $24/Re_p$ to f. With these relations one has ϵ_d as follows from Equation (12):

$$\epsilon_d = \frac{\bar{F}_d}{\bar{u}_t - \bar{F}_c/(1-\epsilon_d)} = \frac{15.3\,\bar{F}_d\,\psi^{3.4}}{1 - \dfrac{\bar{F}_c/(1-\epsilon_d)}{\bar{u}_t}} \tag{14}$$

Since $\bar{F}_d$ is maintained at a constant rate of 0.043 cc./sq. cm. sec. for the runs to measure the mean drop sizes, Equation (14) is transformed to

$$\epsilon_d/F_d^{2/3} = \frac{5.3\,\psi^{2.4}}{1 - \bar{F}_c/\bar{u}_t\,(1-\epsilon_d)} \tag{15}$$

For the Allen region experimental f is easily available. When one applies Equation (9) to d_p for the region of $\omega l/L_o^{1/3} > 1.2$ and the relation $\bar{d}_p = 7.5\ 10^{-2}\ (\omega l/L_o^{1/3})^{-0.6}$ for the region of $\omega l/L_o^{1/3} > 1.2$, $\bar{u}_t$ is calculated from Equation (13). With the procedure the same as that utilized to derive Equation (15), $\epsilon_d/F_d^{2/3}$ is able to be calculated for the Allen region.

$\epsilon_d/F_d^{2/3}$ thus calculated is obviously influenced by $\bar{F}_c$ and is shown in Figure 4 for the flow rates of 0.27 and 0 cc./sq.cm. sec. for $\bar{F}_c$. Experimental $\bar{F}_c$ ranges from 0 to 0.49 cc./sq.cm. sec. Within the accuracy of the data correlated here, however, the influence of $\bar{F}_c$ on $\epsilon_d/F_d^{2/3}$ does not seem noticeable in accordance with the observation by other investigators (*15, 27*). Beyond a certain value of ψ, about 0.4 for the present case, $\epsilon_d/F_d^{2/3}$ begins to deviate from the curve for $\bar{F}_c = 0.27$ and approaches gradually that for $\bar{F}_c = 0$.

Klee and Treybal (*12*) have presented the following empirical correlation to the terminal velocity of a single droplet:

$$u_t = 38.3\,\rho_c^{-0.45}\,\Delta\rho^{0.58}\,\mu_c^{-0.11}\,d_p^{0.70} \tag{16}$$

For the MIBK-water system the correlation is applicable to the range of $Re_p = 20 \sim 300$ and to fairly larger drop sizes than those presented here. In Figure 4 $\epsilon_d/F_d^{2/3}$ calculated from the use of Equations (12) and (16) is also shown for the operating range to which the correlation may be applicable.

It is seen from the above discussion that the holdup correlation of liquid droplets as freely travelling solid spheres gives a fairly reasonable approximation to the experimental measurements.

As shown in the same figure, inclusion of the viscosity of the dispersed phase correlates well the droplet holdup data for different liquids systems other than MIBK, where the continuous phase is always water. The underlying reason is not known definitely. One possible explanation is that liquid jets issuing from the plate perforations during pulsation constitute a kind of Couette type of shear-flow field between the expanding jet in the direction of pulsation and the surrounding fluid flowing in the reverse direction with the jet to compensate the fluid entrained by the jet. As shown by Taylor (*30*), Tomotika (*33*), and Hinze (*9*), droplet dispersion in a shear-flow field is also governed by the ratio μ_d/μ_c. When the ratio is lower than 2, droplets are apt to break up more easily with increasing the ratio, and vice versa when the ratio is greater than 2. The ratios for the liquid-liquid systems correlated in Figure 4 are smaller than 2, except for the water iso-amyl alcohol system utilized by Cohen and Beyer (*5*). μ_d/μ_c for this particular system is about 4.5 at the operating temperature, and the behavior deviates noticeably from the correlation, Equations (6) and (7), as shown in the same figure.

CONCLUSIONS

1. The longitudinal dispersion coefficient for a continuous phase is shown to follow the backflow model and is correlated as Equations (4) and (5).
2. The physical meaning of β is shown to come from the vortex formation due to inherent instability of fluid motion in a compartment.
3. The longitudinal dispersion coefficient for dispersed phase is shown to follow to the velocity distribution mechanism under weak pulse intensity, but the coefficient tends to approach that of the continuous phase with increasing pulse intensity.
4. Droplet holdup is correlated as Equations (6) and (7) for different liquid-liquid systems. The inclusion of dispersed-phase viscosity is necessary to correlate the data successfully.
5. Mean drop size is interpreted mainly on the basis of the rate of energy dissipation in the mixed phases. Holdup correlation based on the assumption that a droplet behaves as a solid sphere at its terminal velocity predicts the empirical data fairly well as shown in Figure 4.

ACKNOWLEDGMENT

The authors express their appreciation for the financial support from the Research Fund (Kagaku-Kenkyūhi) of the Ministry of Education, Japan. They are also grateful for the assistance of Mr. Shinzl Kikuchi during the course of their experimental runs.

NOTATION

C_o = orifice coefficient, dimensionless
c_i = concentration of phase i, mole/cc. ($i = c$ and d)
c^o = feed concentration, mole/cc.
d_h = hole diameter of perforation, cm.
d_p = droplet diameter, cm.
D_T = inside diameter of column, cm.
E_i = superficial longitudinal dispersion coefficient of ith phase, sq. cm./sec. (i = continuous or dispersed)
f = drag coefficient for spheres, dimensionless
f' = volumetric rate of interstage mixing, cc./sq. cm. sec.
F_i = superficial flow rate of ith phase, cc./sq. cm./sec.
l = pulse amplitude, cm.
L = effective column length in the direction of mean flow, cm.
L_o = axial height of one compartment, cm.
m = fraction of total free hole area, dimensionless
n_p = total number of stages, dimensionless
Δp = pressure difference across one plate, g. cm./sq. cm. sec.^{2}
N_{Re_p} = Reynolds number for droplet $= \bar{d}_p\ u_t\ \rho_c/\mu_c$, dimensionless
N_{Re_h} = Reynolds number for orifice $= d_h\ u_h\ \rho_m/\mu_m$, dimensionless
u_d = linear velocity of dispersed phase $= F_d/\epsilon_d$, cm./sec.
u_h = linear velocity of fluid through orifice, cm./sec.

u_t = terminal velocity of a droplet, cm./sec.
z = axial distance, cm.

Greek Letters

β = factor included in Equation (4), dimensionless
β_c = factor included in Equation (A4) $= m^2/(1-m)(1-m^2)$, dimensionless
γ_c = factor included in Equation (A3) $= (1 + L_c/L) 5\pi^2/6\sqrt{2}\, C_c$, dimensionless
ϵ_i = volume fraction of phase i, dimensionless
ϵ_c = rate of energy dissipation per unit mass of mixed phases, sq. cm./sec.^{3}
θ = time, sec.
λ_c = microscale of turbulence, cm.
μ_i = viscosity of phase i, g./cm. sec.
μ_m = viscosiy of mixed phases, g./cm. sec.
ν = kinematic viscosity, sq. cm./sec.
ρ_i = density of phase i, g./cc.
ρ_m = density of mixed phases, g./cc.
$\Delta\rho$ = density difference between dispersed and continuous phases, g./cc.
σ = interfacial tension, dynes/cm.
ω = pulse frequency, cycles/sec.

Subscripts

c = continuous phase
d = dispersed phase
i = ith phase
m = mixed phase

Superscripts

* = calculated value
$\bar{}$ = average value

LITERATURE CITED

1. Aris, Rutherford, and N. R. Amundson, *A.I.Ch.E. Journal*, 3, 280 (1957).
2. Brenner, H., *Chem. Eng. Sci.*, 17, 229 (1962).
3. Burger, L. L., and W. H. Swift, U. S. Atomic Energy Comm., Hanford Works, *Rept. HW-29010* (1953).
4. Chantry, W. A., R. L. Von Berg, and H. F. Wiegandt, *Ind. Eng. Chem.*, 47, 1153 1955).
5. Cohen, R. M., and G. H. Beyer, *Chem. Eng. Progr.* 49, 279 (1953).
6. Damköhler, G., "Der Chemie-Ingenieur," A. Eucken and M. Jackob, ed., Vol. 3, Part 1, p. 366, Akademische Verlagsgesellshaft, Leipzig (1937).
7. Equchi, W., and S. Nagata, *Chem. Eng. (Japan)*, 22, 218 (1958).
8. Endoh, K., and Y. Ōyama, *J. Sci. Res. Inst. No. 1486*, 52, 131 (1958).
9. Hinze, J. O., *A.I.Ch.E. Journal*, 1, 289 (1955).
10. Houston, R. H., *U. S. Atomic Energy Comm., UCRL-3817* (1958).
11. Jealous, A. C., and H. F. Johnson, *Ind. Eng. Chem.*, 47, 1159 (1955).
12. Klee, A. T., and R. E. Treybal, *A.I.Ch.E. Journal*, 2, 444 1956).
13. Latinen, G. A., and F. D. Stockton, Paper presented at A.I.Ch.E. Natl. Meeting, St. Paul, Minn. (September, 1959).
14. Lebenspiel, O., *Ind. Eng. Chem.*, 51, 1431 (1959).
15. Li, W. H., and W. M. Newton, *A.I.Ch.E. Journal*, 3, 56 (1957).
16. Mar, B. W., and A. L. Babb, *Ind. Eng. Chem.*, 51, 1011 (1959).
17. Miyauchi, T., *U. S. Atomic Energy Comm., UCRL-3911* (1957).
18. ———, A. K. McMullen, and T. Vermeulen, *ibid., UCRL-9112* (1960).
19. ———, and H. Ōya, *Chem. Eng. (Japan)*, 27, 322 (1963).
20. ———, Y. Tomura, and T. Vermeulen, unpublished.
21. ———, and T. Vermeulen, *Ind. Eng. Chem. Fundamentals*, 2, 113 (1963).
22. ————, *ibid.* 304.
23. Ōya, H., M.S. thesis, Univ. Tokyo, Tokyo, Japan (1960).
24. Perry, J. H., "Chemical Engineers' Handbook," 3 ed., p. 405, McGraw-Hill, New York (1950).
25. Sato, C., K. Sugihara, and I. Taniyama, *Chem. Eng. (Japan)*, 27, 583 (1963).
26. Sege, G., and F. W. Woodfield, *Chem. Eng. Progr. Symposium Ser. No. 13*, 50, 179 (1954).
27. Sehmel, G. A., and A. L. Babb, *Ind. Eng. Chem. Process Design and Development*, 2, 38 (1963).
28. Shirotuka, M., S. Honda, and Hideo Ōya, *Chem. Eng. (Japan)*, 22, 687 (1958).
29. Sleicher, C. A., Jr., *A.I.Ch.E. Journal*, 5, 149 (1959).
30. Taylor, G. I., *Proc. Roy. Soc.*, A138, 41, (1932), A146, 501 (1934).
31. ———, *ibid.*, A219, 186 (1953). A223, 446 (1954).
32. Thornton, J. D., *Trans. Inst. Chem. Engrs.*, 35, 316 (1957).
33. Tomotika, S., *Proc. Roy. Soc.*, A150, 322 (1935), A153, 302 (1936).
34. Vanderveen, J. H., *U. S. Atomic Energy Comm., UCRL-8733* (1961).
35. Van Dijck, W. J. D., *U. S. Patent 2, 011, 186* (Aug. 13, 1935).
36. Vermeulen, T., G. M. Williams, and G. E. Langlois, *Chem. Eng. Progr.*, 51, 85 (1955).
37. Yagi, S., and T. Miyauchi. *Chem. Eng. (Japan)*, 17, 382 (1953).

APPENDIX

Rate of Energy Dissipation in a Pulsed Perforated Plate Column

Jealous and Johnson (*11*) have treated the power necessary to operate a pulsed perforated-plate column, dividing the power into three categories of static head, inertia of liquid, and friction loss. They calculated the friction loss, assuming a perforation as an orifice and neglecting the pressure recovery after passing through the orifice. Here, however, the pressure recovery will be corrected as follows to calculate the rate of energy dissipation in the mixed phases.

The pressure loss across an orifice is given approximately by Equation (A-1) (*24*).

$$\Delta p = \frac{(1-m)(1-m^2)}{c_o^2}\,\frac{1}{2}\,\rho u_o^2 \qquad \text{(A1)}$$

where c_o is a function of m and $(Re)_h$, and approaches to 0.61 with increasing $(Re)_h$. The mean rate of energy dissipation ϵ_o per unit mass of column fluid is expressed as follows, averaging over the whole effective volume of the column:

$$\bar{\epsilon}_o = (L/L_o + 1)\,\Delta p\, m(\pi/4)\, D_T^2\, u_o/\rho\,(\pi/4)\, D_T^2\, L$$

or

$$\bar{\epsilon}_o = \left(\frac{1}{L_o} + \frac{1}{L}\right)\frac{m(1-m)(1-m^2)\,\overline{u_o^3}}{2\,c_o^2} \qquad \text{(A2)}$$

where $\overline{u_o^3}$ is the time mean of the absolute value of u_o^3 and is expressed as follows when the pulse wave is sinusoidal and $\pi\omega l > (|\bar{F}_d| + |\bar{F}_c|)$:

$$\overline{u_o^3} = \frac{5}{3\sqrt{2}}\,\pi^2\,(\omega l/m)^3 \qquad \text{(A3)}$$

From Equations (A2) and (A3)

$$\bar{\epsilon}_o = \frac{\gamma_c}{\beta_c}\,\frac{(\omega l)^3}{L_o} \qquad \text{(A4)}$$

where

$$\gamma_c = \frac{5\pi^2}{6\sqrt{2}}\,\frac{1 + L_o/L}{c_o}$$

(when $L_o/L << 1$, γ_o is equal to 9.5 by taking $c_o = 0.61$)

$$\beta_c = m^2/(1-m)(1-m^2)$$

Manuscript received June 30, 1964; revision received November 9, 1964; paper accepted November 11, 1964.